Tide-surge interaction off the east coast of Canada and northeastern United States

N. B. Bernier[1] and K. R. Thompson[1]

Received 30 June 2006; revised 21 December 2006; accepted 23 January 2007; published 13 June 2007.

[1] Sea level observations and a dynamical model are used to investigate tide-surge interaction in the coastal waters off the east coast of Canada and northern USA. The study is motivated in part by the need to improve operational forecasts of total water level and coastal flooding. Two statistical methods are used to search for evidence of tide-surge interaction in hourly sea level records from 23 coastal locations. The methods are based on comparison of the statistical properties of the sea level residuals (observed sea level minus tide) occurring at different stages of the tidal cycle. While recognizing the limitations of such an approach, it is concluded that tide-surge interaction does occur in the Northumberland Strait which is located in the southern Gulf of St. Lawrence. Results for the Gulf of Maine and Bay of Fundy are less conclusive. A dynamical model is also used to quantify tide-surge interaction in the study region and to identify its physical causes. Tide-surge interaction in the model is strongest in the Northumberland Strait where the amplitude of the effect can reach 20 cm during and following strong storm surge events. This is large enough to be of practical significance in terms of flood forecasting. A series of sensitivity experiments with the model shows that the nonlinear parameterization of bottom stress is the principal contributor to tide-surge interaction.

Citation: Bernier, N. B., and K. R. Thompson (2007), Tide-surge interaction off the east coast of Canada and northeastern United States, *J. Geophys. Res.*, *112*, C06008, doi:10.1029/2006JC003793.

1. Introduction

[2] The study of tide and surge interaction has a long history [e.g., *Godin*, 1972; *Murty*, 1984]. In a pioneering study of the River Thames in the UK, *Rossiter* [1961] showed that tide-surge interaction can affect significantly the amplitude and timing of storm surges. After examination of the larger surges in this system, *Prandle and Wolf* [1978] concluded that tide-surge interaction increases with the amplitude of the surge. They further concluded that tide-surge interaction can significantly increase the magnitude of surges, especially negative and short-lived surges. More recently, *Davies and Lawrence* [1994] have shown that the interaction of tide and wind-induced currents can lead to a significant modification of the amplitude and phase of M_2 due primarily to enhanced turbulence and bed friction. Tide-surge interaction has also been shown to be important in many other regions including the Meghna Estuary in Bangladesh [*As-Salek and Yasuada*, 2001] and along the North Queensland coast of Australia [*Tang et al.*, 1996].

[3] The tides and surges of the northwest Atlantic and its adjacent shelf seas have received a lot of scientific attention as separate phenomena [e.g., *Garrett*, 1972, 1984; *Greenberg*, 1979; *Dupont et al.*, 2002; *Bobanović et al.*, 2005; *Bernier and Thompson*, 2006]. The interaction of tide and surge has received almost no attention. This is, however, becoming a matter for concern because the present operational forecasts of total water level, and thus coastal flooding, for eastern Canada are based on a linear superposition of the predicted tide and forecast surge [*Bobanović et al.*, 2005]. Improvement of our ability to forecast total water levels is one of the primary motivations for this study. We will use a combination of statistical techniques, and dynamically based models, to both quantify and identify the causes of tide-surge interaction in this region.

[4] Two standard statistical methods are used to identify areas where tide-surge interaction is present. In the first method, we compare the probability distributions of the tidal residuals at different stages of the tide using hourly sea level records from 23 tide gauges bordering the northwest Atlantic [e.g., *Murty*, 1984; *Zhang et al.*, 2000]. In the second method, we check if local extrema in the observed tidal residuals tend to occur at a particular phase of the tide [e.g., *Rossiter*, 1961; *Prandle and Wolf*, 1978; *Wolf*, 1981]. We note that both of these statistical methods involve considerable subjectivity in their practical application. We are, however, able to present a coherent picture: Tide-surge interaction is strongest, and significant from a practical perspective, in the Northumberland Strait in the southern Gulf of St Lawrence (a region known to be vulnerable to coastal flooding). We confirm this result using a series of numerical experiments with a shelf circulation model forced by tides at its open boundaries and wind and air pressure at the sea surface.

[1]Department of Oceanography, Dalhousie University, Halifax, Nova Scotia, Canada.

0148-0227/07/2006JC003793

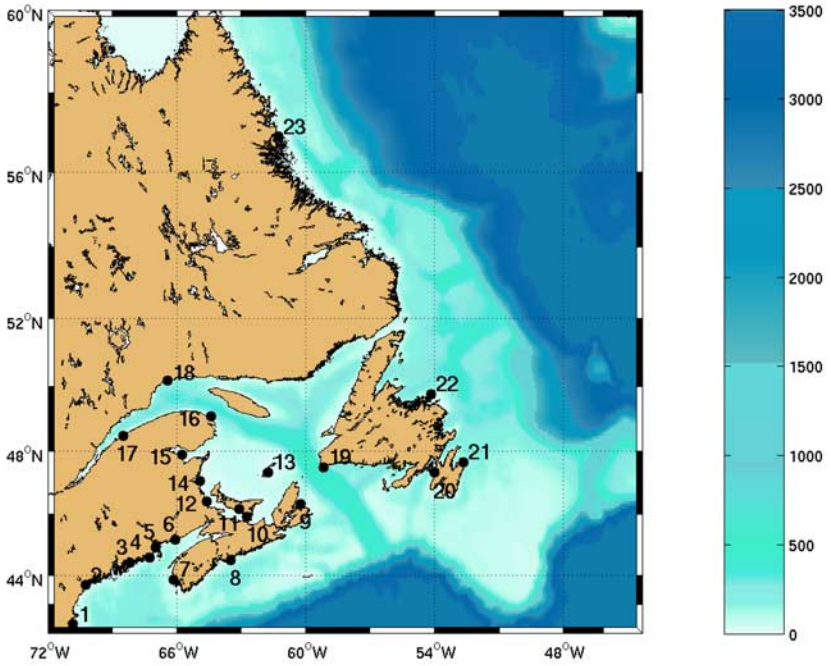

Figure 1. Tide gauge locations and domain of the dynamical model. The domain ranges from 44.33 to 72°W and from 42 to 60°N. The dots show the location of tide gauges used to validate the tide-surge model. The model is tidally forced at the southern, eastern, and northern boundaries, the head of the St. Lawrence River, and the head of the Bay of Fundy. The color bar is the water depth in meters. Note that stations 10, 11, and 12 are located in the Northumberland Strait (the body of water that separates New Brunswick and Nova Scotia from Prince Edward Island).

[5] The outline of this paper is as follows. The sea level observations used to identify areas of tide-surge interaction, and also to validate the model, are described in section 2. The dynamical model is described in the same section. In section 3, the observation records are statistically analyzed to identify tide gauges providing significant evidence of tide-surge interaction. In section 4, the dynamical model is used to quantify, and understand the reasons for, tide-surge interaction. Results are summarized and discussed in section 5.

2. Description of the Sea Level Observations and the Dynamical Model

[6] We now introduce the sea level observations and the dynamical model. We also quantify the ability of the model to predict tides and surges using the sea level observations for validation.

2.1. Sea Level Observations

[7] The observations used in this study were collected in 2005 at 23 tide gauges located along the east coast of Canada and the northeastern USA (Figure 1 and Table 1). The Canadian data were provided by the Marine Environmental Data Service (http://www.meds-sdmm.dfo-mpo.gc.ca), and the US data were downloaded from the Center for Operational Oceanographic Products and Services (http://www.tidesandcurrents.noaa.gov/). Mean sea level was removed from each observation record. All tidal analyses discussed in this paper were performed using t_tide, the MATLAB tidal package of *Pawlowicz et al.* [2002].

2.2. The Dynamical Model

[8] The tide-surge model is a modified version of the Princeton Ocean Model [*Mellor*, 1998] and is based on the following depth-averaged barotropic momentum and continuity equations:

$$\frac{\partial \mathbf{u}}{\partial t} + \mathbf{u}\cdot\nabla\mathbf{u} + \mathbf{f}\times\mathbf{u} = -g\nabla\eta_{\mathrm{WT}} + A\nabla^2\mathbf{u} + \frac{\boldsymbol{\tau}_{\mathrm{s}} - \boldsymbol{\tau}_{\mathrm{b}}}{\rho \mathrm{H}} \quad (1)$$

$$\frac{\partial \eta_{WT}}{\partial t} + \frac{\partial (Hu)}{\partial x} + \frac{\partial (Hv)}{\partial y} = -\frac{\partial \eta_{\mathrm{P}}}{\partial t} \quad (2)$$

where $\mathbf{u} = (u, v)$ denotes the depth-averaged horizontal velocity, $\mathbf{f}$ is the upward pointing unit vector scaled by the Coriolis parameter, $\boldsymbol{\tau}_{\mathrm{s}}$ and $\boldsymbol{\tau}_{\mathrm{b}}$ are the surface and bottom stress, respectively, A is the horizontal viscosity, and H is the total water depth. Note that the sea level has been split into two components: η_P is the inverse barometer effect due to air pressure, and η_{WT} is the isostatically adjusted water level (due primarily to the effect of wind and tides, hence the subscripts). It follows that the total water level is given by $\eta_{WPT} = \eta_{WT} + \eta_P$. The rest of the notation is standard.

[9] The model has five open boundaries: the head of the Bay of Fundy, the head of the St. Lawrence River, and the northern, southern, and eastern limits of the domain (Figure 1). The model has a resolution of 1/12° (corresponding to a latitudinal resolution of about 9 km).

[10] The bottom stress formulation is of the form $c_{db}\mathbf{u}(u^2 + v^2)^{1/2}$ where c_{db}, the bottom drag coefficient, is set equal to 2.5×10^{-3}.

Table 1. Tide Gauge Locations and Hindcast Skill of the Surge Model[a]

Station Name	Code	Lat	Lon	RMS error
Boston	1	42.36	71.05	7.17
Portland	2	43.66	70.25	6.72
Bar Harbor	3	44.39	68.21	6.36
Cutlet Naval Base	4	44.64	67.29	6.16
Eastport	5	44.90	66.99	6.84
Saint John	6	45.25	66.06	7.95
Yarmouth	7	43.84	66.12	11.19
Halifax	8	44.66	63.58	6.41
North Sydney	9	46.22	60.25	7.61
Wood Island	10	45.90	62.75	8.48
Charlottetown	11	46.23	63.11	9.42
Shediac Bay	12	46.23	64.55	10.37
Ile d'Entrée	13	47.28	61.72	6.51
Lower Escuminac	14	47.08	64.88	8.20
Belledune	15	47.90	65.85	8.45
Rivière-au-Renard	16	49.00	64.38	7.61
Pointe-au-Père	17	48.52	68.47	7.52
Sept-Iles	18	50.22	66.40	6.53
Port-aux-Basques	19	47.57	59.13	6.25
Argentia	20	47.30	53.98	8.63
St John's	21	47.57	52.72	6.99
Joe Batts Arm	22	49.73	54.17	7.12
Nain	23	56.55	61.70	8.03

[a]Description of tide gauges used in this study and surge hindcast statistics. The columns are (1) station name, (2) station code, (3) latitude in degrees, (4) longitude in degrees west, and (5) RMS of the surge hindcast error (in cm). The location of the gauges are shown in Figure 1.

[11] A standard radiation condition [e.g., *Davies and Flather*, 1978] is applied at all open boundaries of the model domain. The condition is given by

$$u - u_T = \pm\sqrt{\frac{g}{h}}(\eta - \eta_T) \tag{3}$$

where u_T denotes the tidal currents normal to the boundary, η_T denotes the tidal elevation, and h is the mean water depth. The sign is chosen to ensure that waves approaching the boundary radiate outward. Results from a tidal prediction model (WebTide [*Dupont et al.*, 2002]) are used to specify the tidal currents and elevations along the open boundaries. The tidal forcing is a linear combination of the five dominant diurnal and semidiurnal constituents for this region: O1, K1, M2, N2, and S2 [*Dupont et al.*, 2002].

[12] The surface wind stress is computed from the 10 m wind. The kinematic stress magnitude is given by $c_d(W)W^2$ where W is the wind speed and c_d is a drag coefficient that equals 1.2×10^{-3} for $W < 8$ m s^{-1} and thereafter increases linearly by 0.065×10^{-3} for every 1 m s^{-1} increase in W. The atmospheric forcing was obtained from GEM15, a high spatial resolution (15 km) operational forecast model run by Environment Canada [*Côté et al.*, 1998a, 1998b; *Yeh et al.*,

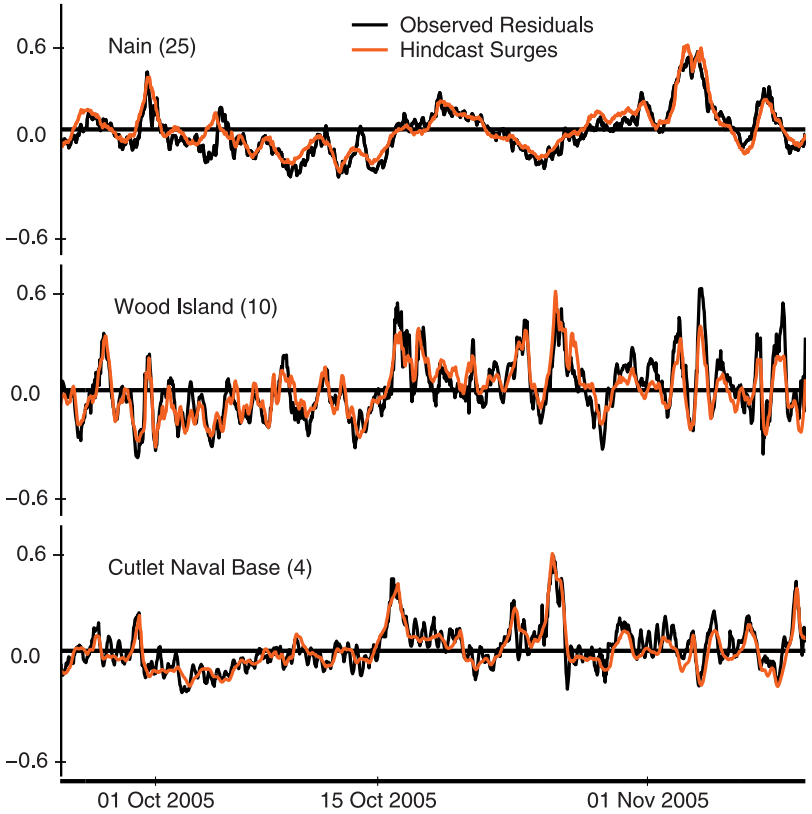

Figure 2. Observed and hindcast storm surges (in m). The black line shows the observed residuals at three representative stations. The red line shows the hindcast surges. All series show that the model captures the rapid changes in sea level associated with storm events and that the overall spectral content of the hindcast surges and observed residuals is similar.

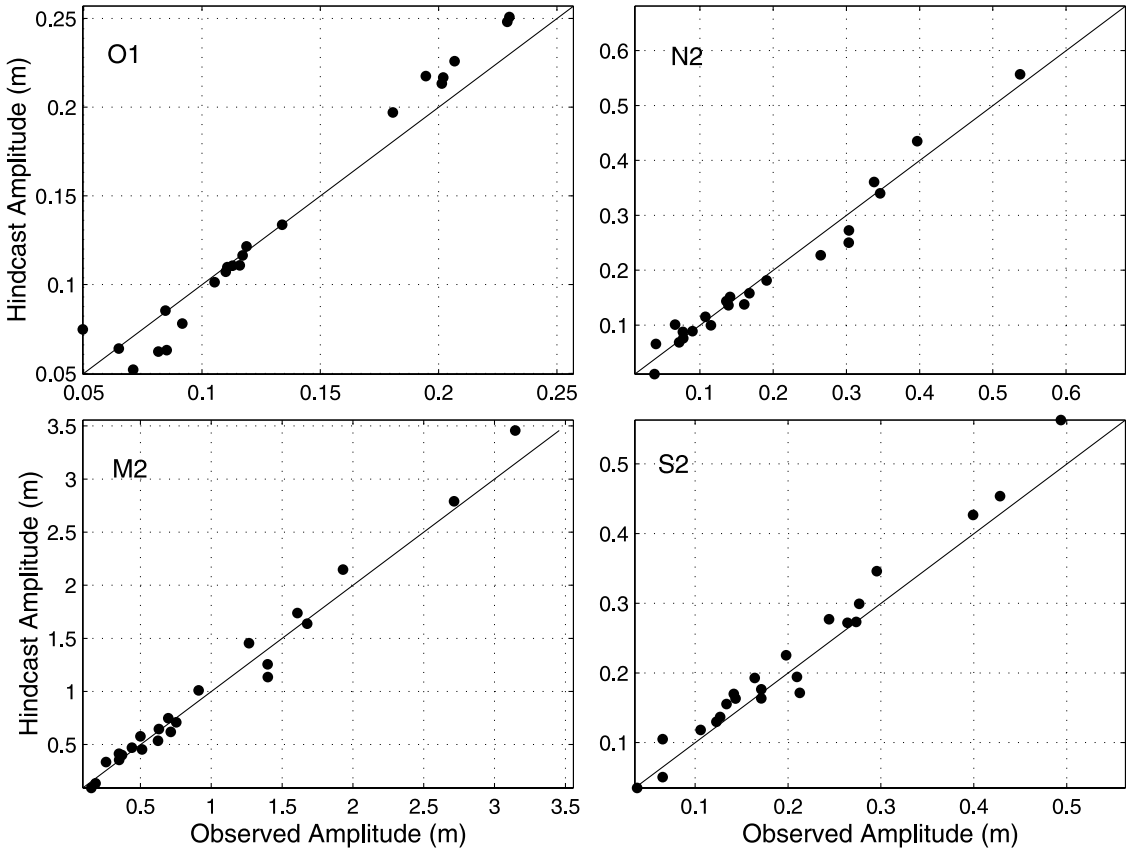

Figure 3. Comparison of the observed and hindcast tidal amplitudes at the 23 tide stations shown in Figure 1. The top left panel is for O1, the top right panel is for N2, and the bottom left and right panels are for M2 and S2, respectively. In general, the observed and modeled amplitudes are within 10 cm for M2 and a few centimeters for the other constituents.

1998]. The wind and air pressure fields were provided with a time spacing of 1 hour.

2.3. Validation of the Dynamical Model

[13] The ability of the model to hindcast tides and storm surges is now checked by comparing model output to the observed sea level records.

[14] Storm surges: The model was run for 2005, driven by hourly surface winds and air pressures. (Tidal forcing was not included at the open boundary.) Hindcast hourly surges (η_{WP}) were then compared directly against observed residuals η_R (observed hourly sea levels after removal of the predicted tide calculated using the tidal package of *Pawlowicz et al.* [2002]).

[15] Overall, there was generally good agreement between the surge hindcasts and the observed residuals. Typical results are shown in Figure 2; the standard deviation of the hindcast error for all stations is given in Table 1. The RMS of the hindcast error is generally less than 8 cm. Note that the hindcast error for Yarmouth is larger primarily because of numerous gaps in the 2005 record and a possible datum shift.

[16] This is the first time to our knowledge that a storm surge model for eastern Canadian waters has been forced with hourly winds and pressure fields. (Normally the fields are provided every 3 or 6 hours.) Previous analyses [e.g., *Bobanović et al.*, 2005; *Bernier and Thompson*, 2006] reported typical RMS errors of 8–10 cm. In these earlier studies, the observed residuals were low-pass filtered to remove energy at period of 12 hours or less. Without such filtering, typical RMS errors would be larger. In the present study, the RMS is smaller, although low-pass filtering was not applied. On the basis of this 1-year analysis, we conclude that the shift to atmospheric forcing with higher temporal resolution has led to a significant reduction in the RMS hindcast error.

[17] Tides: The model was next forced with tidal elevations and tidal currents along the open boundaries for 2005 (the wind and pressure forcing was set to zero). The amplitude and phase of the five dominant tidal constituents were then calculated from the model output using t-tide and compared against the amplitude and phase calculated from the sea level observations.

[18] The observed and predicted tidal amplitudes for the four largest constituents are shown in Figure 3. Overall, there is good agreement in amplitude (typically within 10 cm), suggesting that the model is capable of reproducing the observed tidal variations. We were encouraged to find that, overall, the agreement is comparable to that of WebTide, the source of the open boundary tidal forcing. The maximum tidal amplitude at every grid point for the period 1 February to 15 March 2005 is shown in the upper panel of Figure 4. The maximum tidal amplitude is also plotted for each tide

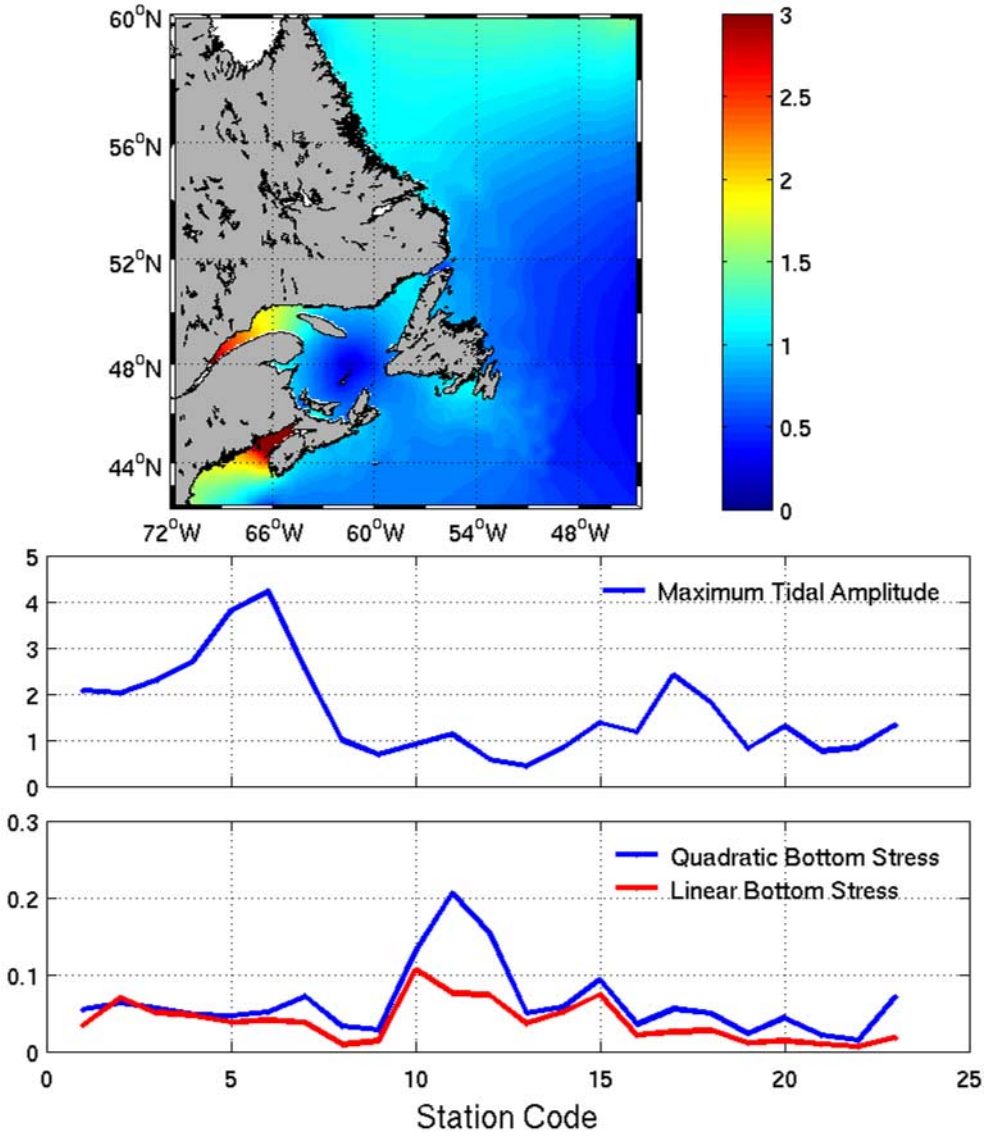

Figure 4. Maxima of the magnitude of the tide and tide-surge interaction for 1 February to 15 March 2005. The top panel is a map of the maximum of the magnitude of the predicted tide (in m) obtained from the tide-only run. (Note that tidal elevations in some areas far exceed 3 m. The color bar was clipped to allow a better overall view of tidal elevations in the entire region.) The middle panel shows the maximum of the predicted tide (in m) at the 23 stations. Note that station 6 is located in the Bay of Fundy. The bottom panel shows the maximum of the tide-surge interaction signal ($|\eta_{WPT} - \eta_T - \eta_{WP}|$) calculated with the fully nonlinear model (in blue) and with linearized bottom stress (in red).

gauge location. Note the high spatial variability in tidal amplitude with the largest tides occurring in the Bay of Fundy and in the St. Lawrence River. The tidal amplitudes in the Northumberland Strait (stations 10–12) are typically 1 m.

3. Observed Tide-Surge Interaction

[19] The hourly sea level observations are now statistically analyzed for tide-surge interaction using two traditional methods. Both methods compare the residual sea levels at different stages of the tide. In section 3.1, the distributions of the residuals are examined. The timing of the residual extrema is discussed in section 3.2. Following *Murty* [1984] and *Zhang et al.* [2000], the tidal stages are defined as (1) high tide (within 1.5 hours of the tidal maximum), (2) low tide (within 1.5 hours of the tidal minimum), (3) falling tide (from the high to low tidal stage), and (4) rising tide (from the low to high tidal stage).

3.1. Distribution of the Residuals

[20] One common way to test for tide-surge interaction is to compare the histograms of the tidal residuals at different stages of the tide using qq-plots [e.g., *Murty*, 1984; *Zhang et al.*, 2000]. A qq-plot is a graphical way of comparing the shape of two histograms. It is essentially a scatterplot of the sorted residuals. In the absence of tide-surge interaction, a qq-plot of residuals recorded at different tidal stages should fall close to the one-to-one line.

[21] The first step in this analysis is to bin the residuals according to the stage of the tide at which they occur [e.g.,

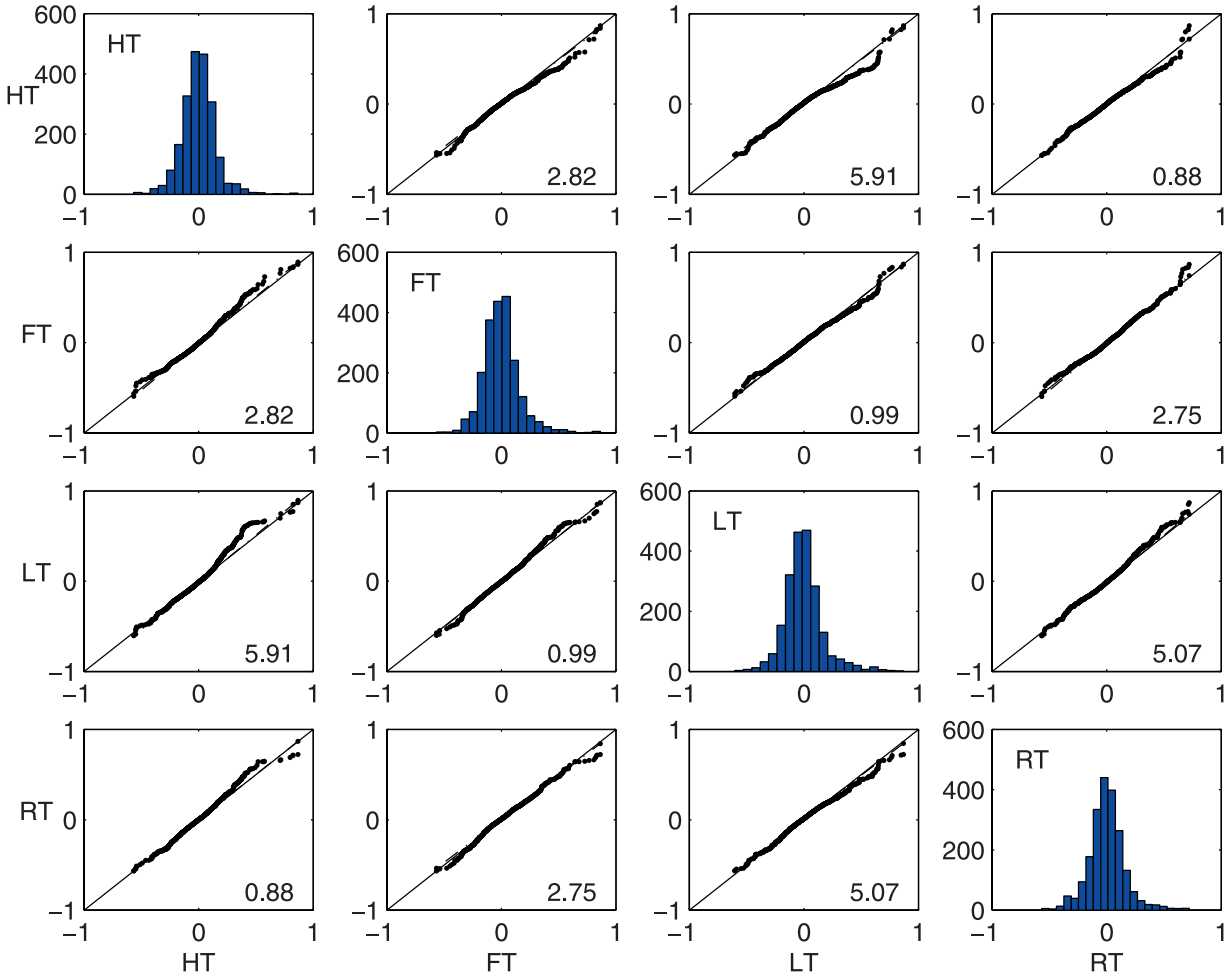

Figure 5. Distribution of the observed residuals at the four stages of the tide for Charlottetown. Observations are for 2005. The four stages are (1) high tide (HT), (2) falling tide (FT), (3) low tide (LT), and (4) rising tide (RT). The diagonal subplots show histograms of the residuals (in m) occurring at a given stage of the tide (*y* axis is the number of residuals in a given bin). The off-diagonal subplots are qq-plots of residual time series (in m). Note qq-plots can only be performed with time series of the same length. The time series used for the qq-plots were based on truncating to the length of the shortest time series. The numbers in the bottom right corner are the Anderson-Darling test statistic (see section 3.1). Values of about 1.99 indicate statistically significant tide-surge interactions at the 10% significance level.

Rossiter, 1961; *Murty*, 1984]. In practice, this is simple at stations dominated by semidiurnal tides. It is not always straightforward at stations with strong diurnal inequality. Our approach was to determine the stage of the tide by visual inspection for problematic cases (i.e., those with strong diurnal inequalities). The next step was to calculate qq-plots of the residuals for all possible pairs of tidal stages. A typical set of qq-plots is shown in Figure 5 for the 2005 observation record from Charlottetown. The diagonal subplots are the histograms of the residuals for the four tidal stages; the off-diagonal panels are qq-plots of the residuals from different tidal stages.

[22] Another problem with this approach is deciding when tide-surge interaction occurs. Visual inspection can be problematic because the eye is immediately drawn to the tails where, by definition, only a small proportion of the data reside. This is illustrated in Figure 5 where, for example, one might conclude that the residual histograms at rising and high tide are different (see top right panel). In an attempt to introduce some objectivity into the assessment of tide-surge interaction, we have used the Anderson-Darling statistic which is based on a tailed-weighted, squared difference of the cumulative distribution functions of the two sets of residuals [*Anderson and Darling*, 1952]. Assuming the observations are independent, the 10% significance level for the test statistic is 1.99. If this value is used to assess the significance of the test statistics (shown in the bottom right corner of each qq-plot), we would conclude that the residual histograms at rising and high tide do not indicate statistically significant tide-surge interaction, in contradiction to our initial visual inspection. This clearly demonstrates the subjectivity inherent in deciding if tide-surge interaction occurs.

[23] To provide an overall impression of tide-surge interaction in each of the 23 sea level records, we have plotted the Anderson-Darling test statistics in Figure 6. Stations

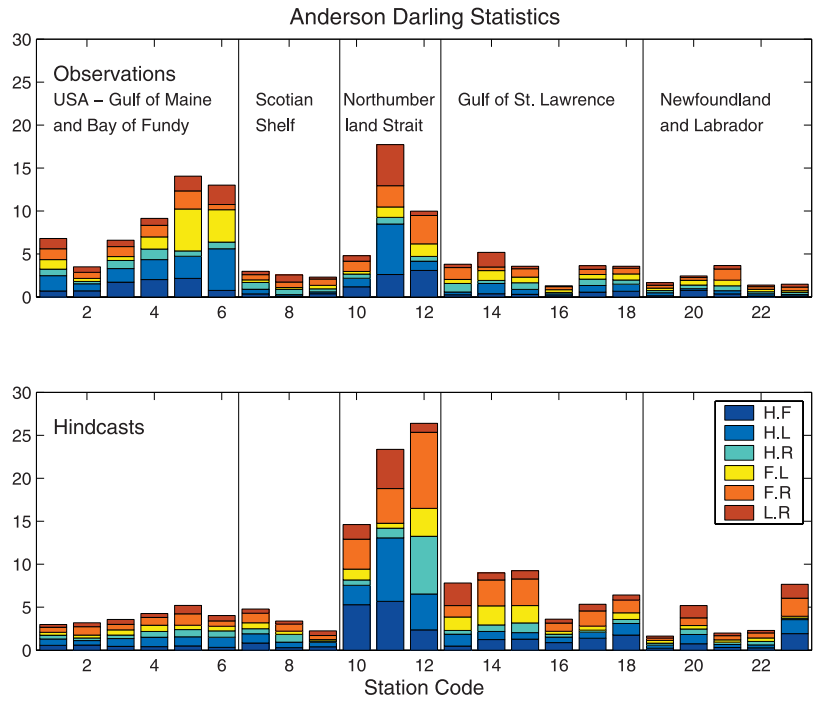

Figure 6. Significance of tide-surge interaction at the 23 tide gauge locations. Top panel shows the Anderson-Darling test statistic for the observed residuals. Bottom panel is the same statistic but for the detided η_{WPT}. The x axis shows the station code. Bars show the Anderson-Darling statistics for all possible pairs of tidal stage (e.g., H. F. are High and Falling Tidal phase pairs; see section 3.1 for details).

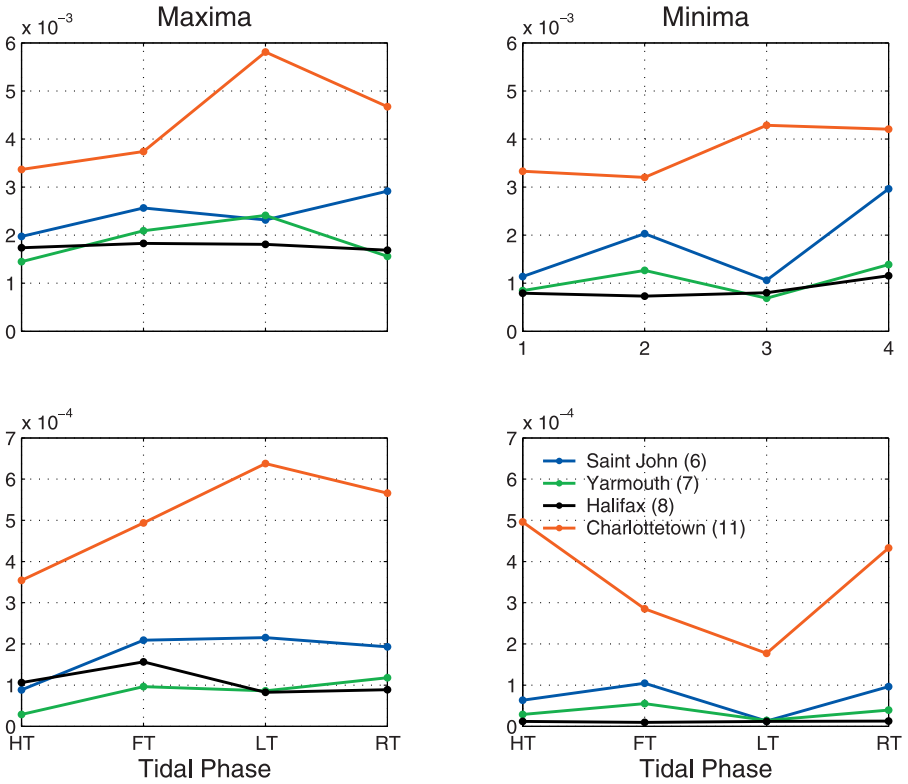

Figure 7. Probability of a storm surge event exceeding a specified threshold for a single hour within a given tidal phase. The x axis marks the tidal phase (see text). The y axis is the probability that a surge event will occur at any hour of a particular tidal stage. Top left panel shows the probability for positive surges larger than 0.3 m. Top right panel is the same but for negative surges less than −0.3 m. Bottom left and right panels are for positive and negative surge beyond 0.6 and −0.6, m respectively. Note that probabilities are based on all available hourly observations between 1960 and 1999.

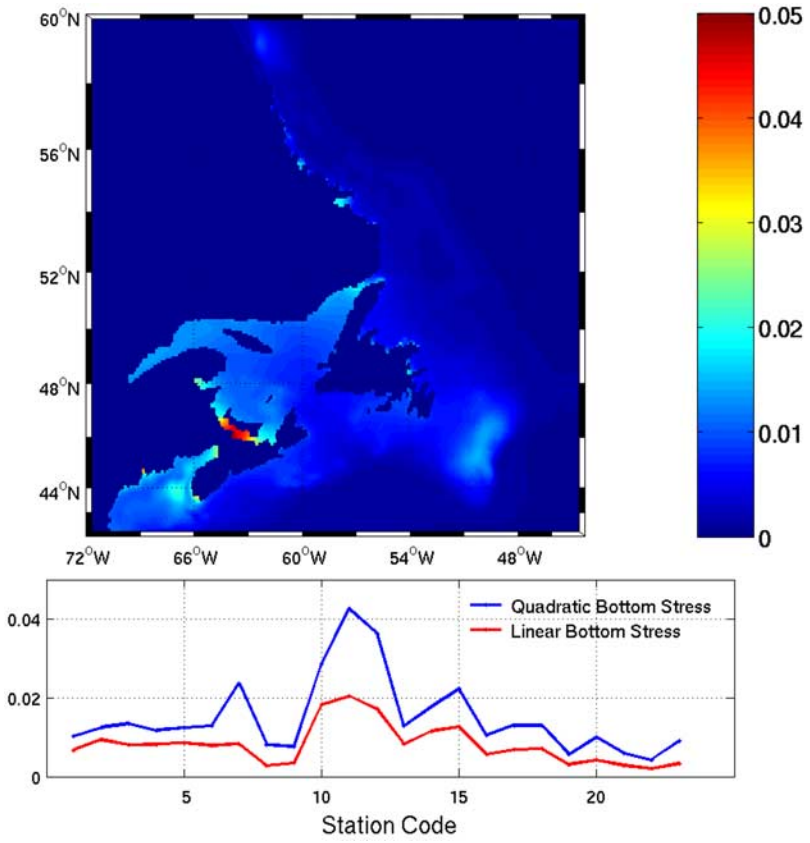

Figure 8. Standard deviation of the effect of tide-surge interaction. Top panel is a map of tide-surge interaction calculated from the fully nonlinear model hindcast. Color bar indicates the standard deviation (in m) of the difference of $\eta_{WPT} - \eta_T - \eta_{WP}$. Bottom panel shows the standard deviation (in m) of the difference of $\eta_{WPT} - \eta_T - \eta_{WP}$ at the 23 tide gauge locations for the fully nonlinear model (in blue) and with linearized bottom stress (in red). Stations with the largest tide-surge interaction signal (10, 11, 12) are located in the Northumberland Strait.

displaying long bars are those with the most significant tide-surge interaction. Overall, the region with the most pronounced tide-surge interaction is the Northumberland Strait (the highest set of bars is for Charlottetown) followed by the Gulf of Maine/Bay of Fundy. It should be noted, however, that the tides of the Bay of Fundy and upper Gulf of Maine are not completely removed by the tidal analysis. This could be due to baroclinic effects that can lead to seasonal variations in the tidal cycle [e.g., *Thompson et al.*, 2007]. It would be possible to remove the tidal remnants by band-pass filtering or further detiding of subblocks of data. Such calculations were not performed in this study because it then becomes difficult to decide if the removal of tidal remnants was in fact due to removal of a true tide-surge interaction signal.

3.2. Timing of Residual Extrema

[24] Another way to test for tide-surge interaction is to compare the probability that a residual extremum (i.e., a local maximum or minimum in time) occurs at a given stage of the tide. In the absence of tide-surge interaction, the probability of an extremum will be approximately equal for each tidal stage.

[25] The first step is to identify the residual extrema that exceed a specified height threshold. To avoid counting the same event twice, the extrema are required to be separated by at least 24 hours. The next step is to calculate the probability that extrema occur at a given stage of the tide (by examining the predicted tidal record around the time of the extreme residual). The probabilities are then adjusted to take into account the different amount of time the tide spends in each of its four stages. The final step is to plot the probabilities, adjusted for the length of the stages, as a function of the stage of the tide and check for differences.

[26] Large surges occur infrequently, and so we have only applied this approach to 11 stations that could provide at least 30 years of hourly sea level data since 1960. The results for surge thresholds of 0.3 and 0.6 m are illustrated in Figure 7 for St. John, Yarmouth, Halifax, and Charlottetown. Note, for example, how minima tend to coincide at falling and rising tide at St. John and Yarmouth, whereas the minima generally occur with equal probability over the tidal cycle at Halifax. We were encouraged to find that the results from the two approaches (probability-based and qq-plots) were broadly consistent: Tide-surge interaction occurs at Charlottetown and possibly the Gulf of Maine/Bay of Fundy.

4. Tide-Surge Interaction in the Dynamical Model

[27] The dynamical model introduced in section 2 is now used to test our conclusion that tide-surge interaction occurs

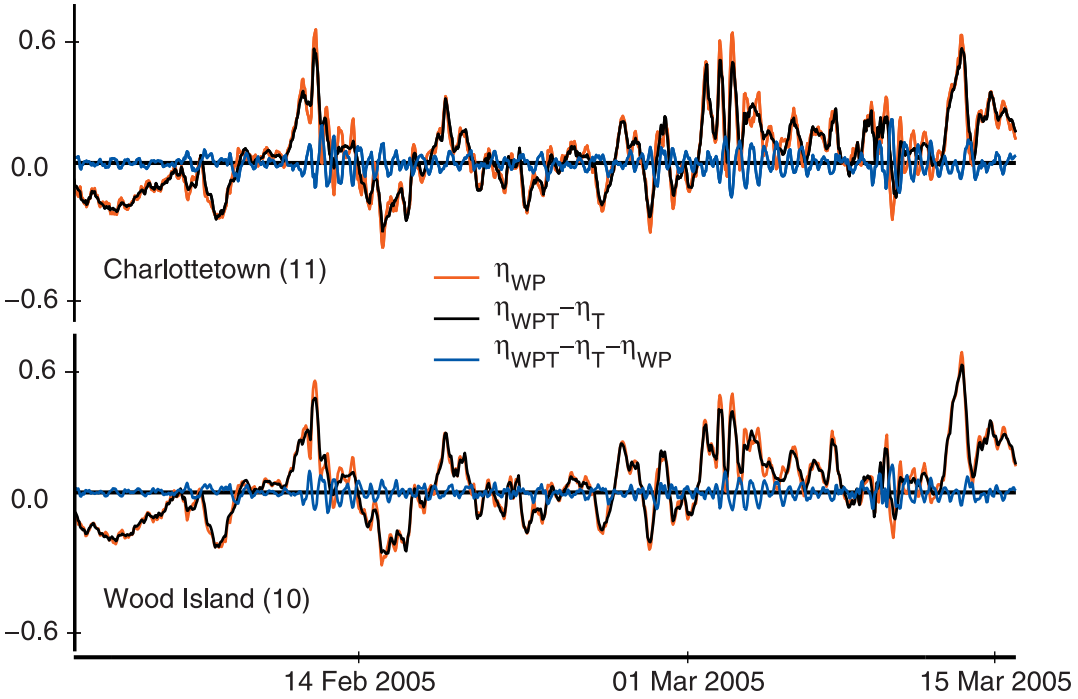

Figure 9. Illustration of the intermittent nature of tide-surge interaction at Charlottetown (top panel) and Wood Island (bottom panel). Black line is $\eta_{WPT} - \eta_T$. Red line is η_{WP}. Blue line is $\eta_{WPT} - \eta_T - \eta_{WP}$ and is due to tide-surge interaction. Note how the amplitude of the blue line is largest when surges are large and rapid, and smallest when the wind- and pressure-driven sea level changes are slow and small.

in the Northumberland Strait and possibly the Gulf of Maine/Bay of Fundy, and, if so, which nonlinear terms in the governing equations (advection or bottom stress in the momentum equation, or tidal pumping in the continuity equation) cause it.

[28] The approach is to run the model separately for 2005 with three different forcing configurations and examine the sea level response. The result of running the model with atmospheric forcing only is denoted by η_{WP}; for tide-only forcing, the result is denoted by η_T. The result of running the model with both atmospheric and tidal forcing is denoted by η_{WPT}. If the model is effectively linear, and tide-surge interaction does not occur, it follows that

$$\eta_{WPT} - \eta_T - \eta_{WP} = 0 \tag{4}$$

We use the difference, $\eta_{WPT} - \eta_T - \eta_{WP}$, as a direct measure of tide-surge interaction.

[29] The above set of three model runs can be repeated with various nonlinear terms either removed or replaced by linear forms. It is then possible to calculate the resulting difference $\eta_{WPT} - \eta_T - \eta_{WP}$ and thus quantify the effect, and cause, of tide-surge interaction.

4.1. Quantifying Tide-Surge Interaction

[30] The top panel of Figure 8 shows the standard deviation of $\eta_{WPT} - \eta_T - \eta_{WP}$ for the fully nonlinear model. Tide-surge interaction is most evident in shallow regions of the domain (see Figure 1 for water depth). The differences are largest around the Northumberland Strait (RMS of 4.5 cm), a region of possible tide-surge interaction identified by the statistical analysis of observed sea level records (see section 3). Regions of secondary importance include the Bay of Fundy, Grand Banks, and Strait of Belle Isle, but the magnitudes of the difference there are small (RMS of about 2 cm).

[31] Because of the nature of the process, tide-surge interaction will only contribute significantly to the total sea level when the surges are large enough to interact. Thus the RMS of the difference is not a good measure of the amplitude of the intermittent products of tide-surge interaction. This is illustrated by the case study shown in Figure 9 for 1 February to 15 March 2005 in the Northumberland Strait. Clearly the effect of tide-surge interaction is intermittent and, for this example, is largest during and immediately following strong storm surge events. It is also clear that the peak amplitude of the interaction effects can reach 20 cm in amplitude (Figure 4).

[32] We also analyzed the time series of η_{WPT} for tide-surge interaction using the qq-plot approach (section 3.1) after removal of the tide using t_tide. Overall, the qq-plots of the detided η_{WPT} compare well with those of the observed records except for the stations in the Bay of Fundy upper Gulf of Maine area. (Figure 10 shows the qq-plots for Charlottetown for comparison with Figure 5.) As mentioned above, the apparent tide-surge interaction in the observation records from this region may be the result of large (10–15 cm) tidal remnants in the residual time series. Elsewhere, the qq-plots of detided η_{WPT} show that the dynamical model is capable of resolving tide-surge interaction.

[33] We also calculated the Anderson-Darling test statistics for the detided η_{WPT} for all possible combinations of tidal stages, in exactly the same way as for the observed

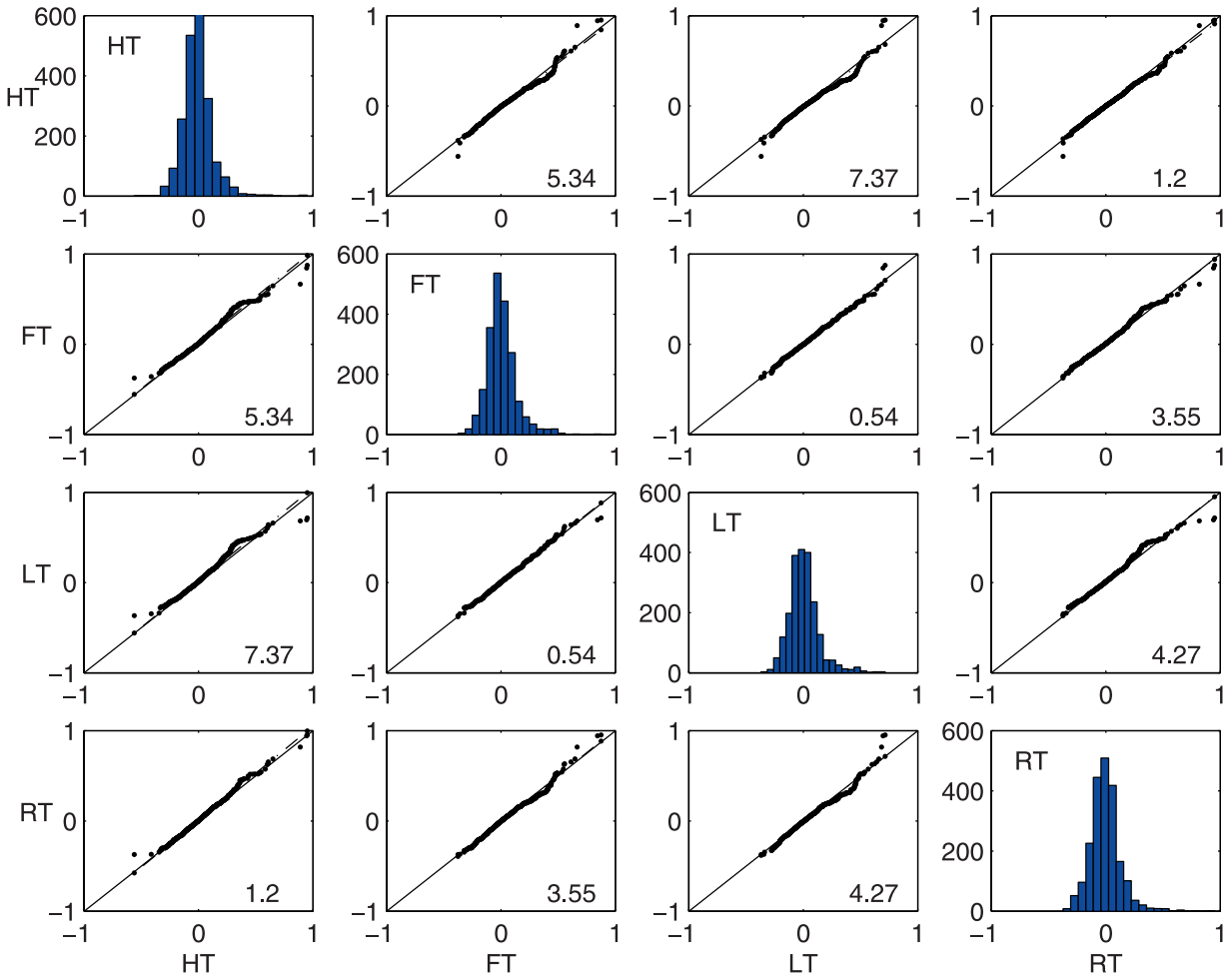

Figure 10. Same as Figure 5 but for η_{WPT} with the tides removed using the t_tide tidal analysis package.

residuals (section 3). The results (Figure 6) are in reasonable agreement with results from the observed residuals (compare top and bottom panels) at all locations except the Gulf of Maine/Bay of Fundy stations.

[34] Overall, we conclude that the model does a reasonable job of reproducing the main features of tide-surge interaction evident in the observations. We now try to identify the cause.

4.2. Causes of Tide-Surge Interaction

[35] The same three hindcasts were repeated with the tidal pumping term linearized such that equation (2) takes the form

$$\frac{\partial \eta_{WT}}{\partial t} + \frac{\partial (hu)}{\partial x} + \frac{\partial (hv)}{\partial y} = -\frac{\partial \eta_P}{\partial t} \tag{5}$$

The effect on the difference, $\eta_{WPT} - \eta_T - \eta_{WP}$, was negligible. (Note that it is possible the pumping term could have a significant effect in a higher-resolution 3D model).

[36] Linearizing bottom friction had a much larger effect on the difference as shown in Figure 8. The standard deviation of the difference is clearly much smaller than for runs with nonlinear bottom stress (red line versus blue line, bottom panel of Figure 8). Overall, linearizing bottom friction reduces the RMS of the differences to below 2 cm at all stations, thereby implying that tide-surge interaction, in this region, is largely due to the nonlinear bottom stress formulation. This is illustrated in Figures 4 and 11 which shows the difference $\eta_{WPT} - \eta_T - \eta_{WP}$ for hindcasts performed using linear bottom friction.

5. Conclusions

[37] Statistical analysis of hourly sea level records from 23 tide gauges bordering the Northwest Atlantic indicates that tide-surge interaction occurs in the Northumberland Strait and possibly the Gulf of Maine/Bay of Fundy. We note, however, that the application of the two statistical methods used in this study is not straightforward; subjective choices (for example, definition of tidal stage, curvature in qq-plots) can be problematic. We attempted to introduce some objectivity by using the Anderson-Darling test statistic to quantify differences in residual histograms for different tidal stages. Again, this test statistic is subjective in the sense that it uses a particular weighting function that focuses attention on the tails of the residual distribution. (It is a modified form of the well-known Kolmogorov-Smirnov test for the equality of two probability distributions.) Such arbitrariness is inevitable when attempting to quantify the differences in two distributions by a single

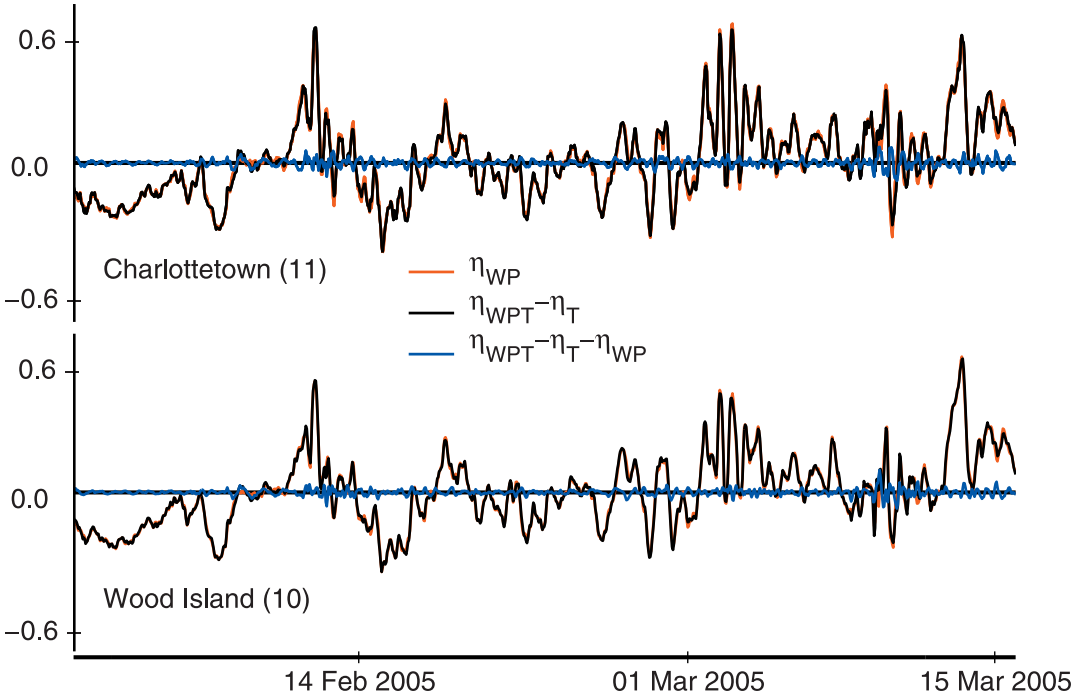

Figure 11. Same as Figure 9 but for a hindcast performed using linearized bottom friction. Note the small remaining tide-surge signal which is primarily due to the nonlinear advection term.

number. Fortunately we found that the two methods generally led us to the same conclusion.

[38] Another problem with standard analyses of tide-surge interaction is that they do not take into account the intermittency of the process. Using the dynamical model, we have shown that the interaction effects in the study region are a function of surge amplitude (in accord with earlier studies [e.g., *Prandle and Wolf*, 1978; *Wolf*, 1981]). Thus measures of tide-surge interaction, based on RMS-type statistics or the shape of residual histograms, will generally underestimate the effect.

[39] Hindcasts of the tides were performed using a depth-averaged nonlinear barotropic model forced by realistic tides along its open boundaries. The predicted amplitude of M2, the largest tidal constituent, is within 10 cm of the observed tidal amplitudes at all tide gauge locations. Amplitudes of the other four largest tidal elevation (O1, K1, N2, and S2) are typically within a couple centimeters of the observed amplitudes.

[40] Storm surge hindcasts were also performed with model forced by hourly surface winds and air pressures. It is interesting to note that the use of hourly forcing, as opposed to the three or six hourly forcing of earlier studies, led to a significant reduction of the RMS hindcast error.

[41] The dynamical model was used to investigate tide-surge interaction by adding a surge-only hindcast to a tide-only hindcast and comparing the sum to a combined tide-surge hindcast. Differences were largest in the Northumberland Strait; regions of secondary importance included the Grand Banks, Gulf of Maine/Bay of Fundy, and the Strait of Belle-Isle. The differences were shown to be primarily the result of the nonlinear bottom stress formulation. This was done by performing the same set of hindcasts with linearized bottom stress and comparing the results with those of the fully nonlinear model.

[42] The results presented in this paper imply that tide-surge interaction is an important process to include in water level forecasts for some locations within the study region. Fortunately it can be readily included in the present operational flood warning system along with more frequent updates of the atmospheric forcing. Such improvements are presently underway.

[43] **Acknowledgments.** We thank the Climate Change Action Fund and the Office of Critical Infrastructure Protection and Emergency Preparedness (OCIPEP) for financial support for the work reported on here. KRT acknowledges financial support from the Discovery Grant Program of the Natural Sciences and Engineering Research Council of Canada (NSERC), and the Canada Research Chairs Program. The authors acknowledge the ongoing help of Environment Canada and, in particular, Serge Desjardins, for assistance in the acquisition of high-resolution wind and pressure fields used in this study.

References

Anderson, T. W., and D. A. Darling (1952), Asymptotic theory of certain goodness-of-fit criteria based on stochastic processes, *Ann. Math. Stat.*, *23*, 193–212.

As-Salek, J. A., and T. Yasuada (2001), Tide-surge interaction in the Meghna estuary: Most severe conditions, *J. Phys. Oceanogr.*, *31*, 3059–3072.

Bernier, N. B., and K. R. Thompson (2006), Predicting the frequency of storm surges and extreme sea levels in the northwest Atlantic, *J. Geophys. Res.*, C10009, doi:10.1029/2005JC003168.

Bobanović, J., K. R. Thompson, S. Desjardins, and H. Ritchie (2005), Forecasting storm surges along the east coast of Canada and the northeastern US: The storm of 21 January 2000, *Atmos. Ocean*, in press.

Côté, J., S. Gravel, A. Méthot, A. Patoine, M. Roch, and A. Staniforth (1998a), The operational CMC-MRB Global Environmental Multiscale (GEM) model: Part I—Design considerations and formulation, *Mon. Weather Rev.*, *126*, 1373–1395.

Côté, J., J.-G. Desmarais, S. Gravel, A. Méthot, A. Patoine, M. Roch, and A. Staniforth (1998b), The operational CMC-MRB Global Environmental Multiscale (GEM) model: Part II—Results, *Mon. Weather Rev.*, *126*, 1397–1418.

Davies, A. M., and R. A. Flather (1978), Application of numerical models of the north west European continental shelf and the North Sea to the computation of the storm surges of November to December 1973, *Dtsch. Hydrogr. Z., Ergänzungsheft, A*, *14*, 72 pp.

Davies, A. M., and J. Lawrence (1994), Examining the influence of wind and wind wave turbulence on tidal currents, using a three-dimensional hydrodynamic model including wave-current interaction, *J. Phys. Oceanogr.*, *24*, 2441–2460.

Dupont, F., C. G. Hannah, D. A. Greenberg, J. Y. Cherniawsky, and C. E. Naimie (2002), Modelling system for tides for the northwest Atlantic coastal ocean, *Can. Tech. Rep. Hydrogr. Ocean Sci.*, *221*.

Garrett, C. (1972), Tidal resonance in the bay of Fundy and Gulf of Maine, *Nature*, *238*, 441–443.

Garrett, C. (1984), Tides and tidal power in the Bay of Fundy, *Euro-Art., Endeavour, New Ser.*, *8*, 58–63.

Gill, A. (1982), *Atmosphere-Ocean Dynamics*, vol. 30, International Geophysics Series, Elsevier, New York.

Godin, G. (1972), *The Analysis of Tide*, University of Toronto Press.

Greenberg, D. A. (1979), A numerical model investigation of tidal phenomena in the Bay of Fundy and Gulf of Maine, *Mar. Geod.*, *2*, 161–187.

Mellor, G. L. (1998), Users guide for a three-dimensional, primitive equation, numerical ocean model. Technical report, Princeton University, Princeton, N. J., 08544-0710.

Murty, T. S. (1984), Storm surges: Meteorological ocean tides, *Can. Bull. Fish. Aquat. Sci.*, *212*, 897 pp.

Pawlowicz, R., B. Beardsley, and S. Lentz (2002), Classical tidal harmonic analysis including error estimates in MATLAB using T_TIDE, *Comput. Geosci.*, *28*, 929–937.

Prandle, D., and J. Wolf (1978), The interaction of surge and tide in the North Sea and River Thames, *Geophys. J. R. Astron. Soc.*, *55*, 203–216.

Rossiter, J. R. (1961), Interaction between tide and surge in the Thames, *Geophys. J. R. Astron. Soc.*, *6*, 29–53.

Tang, Y. M., R. Grimshaw, B. Sanderson, and G. Holland (1996), A numerical study of storm surges and tides, with application to the North Queensland coast, *J. Phys. Oceanogr.*, *26*, 2700–2711.

Thompson, K. R., K. Ohashi, J. Sheng, J. Bobanovi, and J. Ou (2007), Suppressing drift and bias of coastal circulation models through the assimilation of seasonal climatologies of temperature and salinity, *Cont. Shelf Res.*, in press.

Wolf, J. (1981): Surge-tide interaction in the North Sea and River Thames, in *Floods due to high winds and tides*, pp. 75–94, Elsevier, New York.

Yeh, K.-S., J. Côté, S. Gravel, A. Méthot, A. Patoine, M. Roch, and A. Staniforth (1998), The CMC-MRB Global Environmental Multiscale (GEM) Model. Part III: Nonhydrostatic formulation, *Mon. Weather Rev.*, *130*, 339–356.

Zhang, K., B. C. Douglas, and S. P. Leatherman (2000), Twentieth-century storm activity along the U.S. East Coast, *J. Clim.*, *13*, 1748–1760.

N. B. Bernier and K. R. Thompson, Department of Oceanography, Dalhousie University, 1355 Oxford Street, Halifax, Nova Scotia, B3H 4J1, Canada. (natacha.bernier@phys.ocean.dal.ca; keith.thompson@dal.ca)